



Ti-6Al-4V lattices obtained by SLM: characterisation of the heterogeneous high cycle fatigue behaviour of thin walls.

Marie Pirotais, Nicolas Saintier, Charles Brugger, Vincent Conesa

► To cite this version:

Marie Pirotais, Nicolas Saintier, Charles Brugger, Vincent Conesa. Ti-6Al-4V lattices obtained by SLM: characterisation of the heterogeneous high cycle fatigue behaviour of thin walls.. Procedia Structural Integrity, 2022, Fatigue Design 2021, International Conference Proceedings, 9th Edition, 38, pp.132-140. 10.1016/j.prostr.2022.03.014 . hal-03776870

HAL Id: hal-03776870

<https://hal.science/hal-03776870>

Submitted on 14 Sep 2022

HAL is a multi-disciplinary open access archive for the deposit and dissemination of scientific research documents, whether they are published or not. The documents may come from teaching and research institutions in France or abroad, or from public or private research centers.

L'archive ouverte pluridisciplinaire **HAL**, est destinée au dépôt et à la diffusion de documents scientifiques de niveau recherche, publiés ou non, émanant des établissements d'enseignement et de recherche français ou étrangers, des laboratoires publics ou privés.



Distributed under a Creative Commons Attribution - NonCommercial - NoDerivatives 4.0 International License



Available online at www.sciencedirect.com

ScienceDirect

Procedia Structural Integrity 38 (2022) 132–140

Structural Integrity

Procedia

www.elsevier.com/locate/procedia

Fatigue Design 2021, 9th Edition of the International Conference on Fatigue Design

Ti-6Al-4V lattices obtained by SLM : characterisation of the heterogeneous high cycle fatigue behaviour of thin walls.

Marie PIROTAIS^a, Nicolas SAINTIER^a, Charles BRUGGER^a, Vincent CONESA^b

^a*Arts et Métiers ParisTech, I2M, CNRS, Talence 33400 France*

^b*CEA C.E.S.T.A, Le Barp 3314 France*

Abstract

Architected materials are attracting increasing interest since a few years, achieving numerous excellent specific properties compared to fully dense materials. The transport industry sector see periodic assemblies of elementary cells, called lattices, as a solution to lighten structures. This is made possible by the development of Additive Manufacturing technologies (AM). Among the numerous advantages of AM, these processes allow to create a wide range of porous cell topologies, and to tailor their complex geometry with the desired properties. However, understanding their fatigue properties is essential to validate their long-term use in load-bearing parts.

The FA process plays an important role in fatigue life, as it generates residual stresses, heterogeneous microstructure, as well as surface and volume defects (roughness, gaz porosities, lack of fusion porosities), which are preferred sites for fatigue crack initiation. The fatigue life of these structures also depends strongly on their geometry, which, due to their complexity, induces scale and stress gradient effects.

Recent studies have recognize thin-walls TPMS (Triply Periodic Minimal Surfaces) structures as the most promising structures for fatigue resistance, especially the gyroid geometry, compared to conventional strut-lattices.

The first aim of this work is to characterise the major parameters influencing fatigue life at the lattice scale. Roughness, microstructure will be described on a lattice specimen, and topology effect on stress distribution will be numerically quantified. In order to understand the influence of these parameters, and identify the critical region for fatigue life, this work focuses on the local thin-wall scale. Here, the aim is to characterise the high cycle (HCF) fatigue heterogeneous response of Ti-6Al-4V thin-walls manufactured, characterising locally the HCF behaviour of a TPMS lattice structure ($R=0.1$; uniaxial tension loading, $N=1.10^6$, $f=40\text{Hz}$).

© 2021 The Authors. Published by Elsevier B.V.

This is an open access article under the CC BY-NC-ND license (<https://creativecommons.org/licenses/by-nc-nd/4.0>)

Peer-review under responsibility of the scientific committee of the Fatigue Design 2021 Organizers

Keywords: Selective Laser Metling; Ti-6Al-4V; Lattices; HCF; roughness; microstructure; thin-wall

E-mail address: marie.pirotais@ensam.eu

1. Introduction

AM technology allows a considerable gain in part mass, in production costs, in functional performance and in realization compared to classical subtractive processes. The acquisition of knowledge on the mechanical properties of AM parts will allow to rethink the design and the manufacture of generic parts in the fields of medicine, automobile, aeronautics and space industry (Hannibal et al., 2018).

Among the AM processes, Selective Laser Melting (SLM) allows to reach the special resolution requested for small scale structures, with high geometry quality manufacturing and of superior mechanical properties parts (Yuan et al., 2019). However, a number of technological drawbacks limit the use of AM parts in a fatigue context. Although applying a Hot Isostatic Pressure treatment limits the presence of pores, unmelted particules and residual stresses (Masuo et al., 2017; Tammas-Williams et al., 2017), surface roughness and geometrical imperfections, inherent to the process (Stef et al., 2018), behave like notches where the stress concentration leads to an early crack initiation (Vayssette, 2020). The printing quality depends on many parameters such as heat density, laser path strategy (Speirs et al., 2017) and misorientation between normal to surface and BD (downskin/up-skin effect). Therefore, the characterisation of parameters influencing the fatigue behaviour is essential to validate their long-term use in load-bearing parts.

The development of light 3D-periodic structures named lattices, is directly linked with the AM booming. These architected structures are attracting increasing interest since a few years, achieving numerous excellent specific properties compared to fully dense materials. Their development opens up new perspectives of complex and multi-scale parts, introducing new material properties domains. Such structures are developed for biomedical implants (Yuan et al., 2019; Attaran et al., 2017; Dallogo et al., 2019), lightweight structures for the transport (Gu et al., 2021), heat exchangers (Kaur et al., 2021), catalyst for chemical use (Innocentini et al., 2019), or energy absorption parts (Xiang et al., 2019). Therefore, lattices are the subject of particular attention in the recent literature.

Among all lattices, the gyroid sheet-lattice has recently been experimentally identified as the best candidate for high HCF resistance, showing a better HCF behaviour compared to conventional strut-lattices (Speirs et al., 2017; Bobbert et al., 2017; Refai et al., 2019). This behaviour is explained by its particular topology, allowing a good manufacturing quality (Bobbert et al., 2017), minimizing stress concentrations (Yang et al., 2019; Bobbert et al., 2017; Refai, 2020; Yang et al., 2019).

This work investigates at first the parameters causing an heterogeneous HCF behaviour within the Ti-6Al-4V gyroid thin-wall (TWL) lattice, manufactured by Selective Laser Melting, and post-treated by HIP. Besides, a FEM numerical approach is developed to predict the multiaxial stress field of the structure under loading. A fatigue post-computation of these results allows to predict fatigue critical areas using a local multi-axial fatigue criterion. Having HCF influence parameters identified at the lattice scale, this work aims as a second step to characterize the HCF behaviour heterogeneity of non-architected thin-walls specimens (TWS) describing the local behaviour over the lattice unit cell, and thus demonstrating the anisotropy of TWL.

2. Material and Method

2.1. Samples conception

2.1.1. Gyroid thin-wall lattices

The mathematical approximation (eq. 1) describes the gyroid TPMS, with x, y, z the coordinate points, A the scale factor to control cell periodicity defined as $A = \frac{2*\pi}{L}$ and L the dimension of the unit cell. Its deviation from the exact formulation is minimal compared to the SLM printing quality. No classical computer-aided design software allow to generate the parametric surfaces defined by an implicit equation. Hence, the cells were created by generating two surfaces with the contour3D function of the python's mayavi2 package. Therefore, equation 1 is modified adding a thickness parameter e equals to 300 μm (eq. 2). Surfaces are created over $(n_x \cdot L, n_y \cdot L, n_z \cdot L)$ domain with (n_x, n_y, n_z)

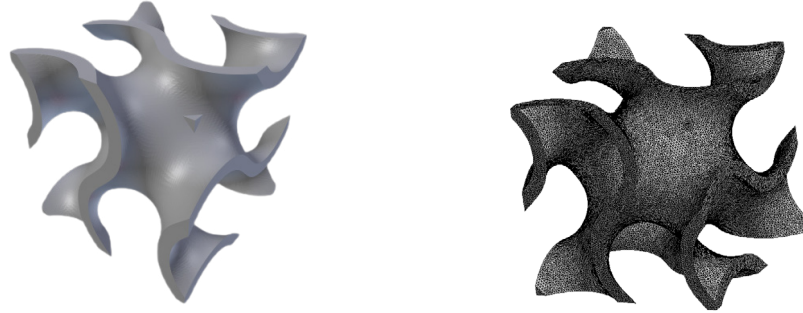


Fig. 1: Gyroid sheet lattice unit cell (4*4*4mm) and its mesh.

, $n_z) = (1, 1, 1)$ for a gyroid TWL unit cell. Finally, the closure of volume is carried out with Materialize MAGICS (fig. 1).

$$\cos(A.x).\sin(A.y) + \cos(A.y).\sin(A.z) + \cos(A.z).\sin(A.x) = 0 \quad (1)$$

$$\cos(A.x).\sin(A.y) + \cos(A.y).\sin(A.z) + \cos(A.z).\sin(A.x) \pm \frac{e}{2} = 0 \quad (2)$$

2.1.2. Thin-wall specimens

Tubular thin-wall specimens are manufactured to characterize the local anisotropic behaviour of the gyroid TWL. Because of their tubular geometry, the TWS do not follow the classical standards HCF samples geometry (fig. 2). The stress concentration coefficient K_t is estimated by FEA. In this study, two parameters of influence are investigated : thickness ($e=\{300, 500\}\mu\text{m}$) and TWS orientation with respect to the SLM plate ($\theta=\{90, 45\}^\circ$).

2.2. Additive manufacturing and post-processing

TWL and TWS are manufactured by SLM on the SLM-280-HL machine (titanium plate, argon atmosphere, Ti-6Al-4V standard strategy), using Ti-6Al-4V ELI (grade 23) powder with a particle diameter of 20-63 μm (SLM Solution) and a chemistry according to ASTM B348/F136 (tab. 1). The SLM as-build (AB) surface aspect is conserved.

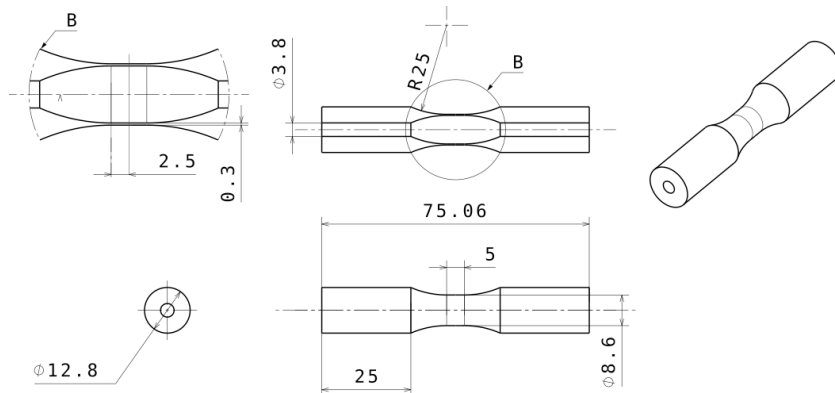


Fig. 2: Geometry and dimension of thin-wall specimens.

Table 1: Ti-6Al-4V ELI chemical composition.

Element	Al	V	Fe	C	N	O	H	Ti	Total Other
wt[%]	6,47	3,9	0,22	0,02	0,01	0,09	0,0017	Base	<0,4

All samples were post-processed by Hot Isostatic Pressing (HIP) at 920°C, under 1020MPa, during 2 hours (argon atmosphere) to enhance mechanical properties (microstructure, internal pores closure, release of residual stress). The effectiveness of HIP on thin-wall lattices has been verified by micro-tomography RX.

2.3. HCF testing

TWS were tested in uniaxial tension ($R=0,1$) up to failure. Fatigue tests were conducted on hydraulic fatigue machine (MTS), with load control, using a sinusoidal waveframe at a frequency of 40Hz, at room temperature and air. Short staircase tests were performed before completing the Whöler curve. For confidentiality reasons, all results are normalised by an arbitrary value

2.4. HCF numerical simulations

To characterise the stress field, a FEM calculation is conducted using Zebulon code (ONERA-Mines Paris) considering a gyroid TWL unit cell (2 249 392 elements). Its behaviour is assumed to be strictly elastic isotropic with $E = 110$ GPA and $\nu = 0.34$. Periodic limit conditions are imposed, and the uniaxial tension load along Z equals to the experimental fatigue life of gyroid lattices (uniaxial tension, $R=0,1$, $N=1.10^6$ cycles, $\sigma_d = 23.4$ MPa). A fatigue post-computation of these results allows to predict critical areas. A local multi-axial fatigue criterion (Crossland) is chosen to consider the fatigue stress field heterogeneity (eq. 3). Fatigue coefficients result from a previous work on as-build bulk Ti-6Al-4V SLM HIPed specimens Vayssette (2020), and are from HCF fully reverse traction/compression and torsion experiments ($\alpha = 0.707$ and $\beta = 195.2$ MPa). As HCF results, numerical results are normalised by the same arbitrary value.

$$FIP_{CR} = \tau_{oct,a}(M) + \sigma_{H,max}(M) \leq \beta \quad (3)$$

$$\sqrt{J_{2,a}} = \max_{t \in T} \|\underline{\underline{S}}(t) - \underline{\underline{S}}_m\| = \max_{t \in T} \sqrt{\frac{1}{2} \left[\underline{\underline{S}}(t) - \underline{\underline{S}}_m \right] : \left[\underline{\underline{S}}(t) - \underline{\underline{S}}_m \right]} \quad (4)$$

$$\underline{\underline{S}}_m = \min_{t \in T} \left(\max_{t \in T} \|\underline{\underline{S}}(t) - \underline{\underline{S}}'\| \right) \quad (5)$$

$$\sigma_{H,max} = \max_{t \in T} \left[\frac{1}{3} \text{tr} (\underline{\underline{\sigma}}(M, t)) \right] \quad (6)$$

3. HCF influence parameters for lattice structures

3.1. Surface roughness

Surface roughness is observed with 2D optical analysis on the X-BD section of embedded TWL lattice samples (fig. 3). Although the gyroid TWL topology allows a good printing quality (well self-supported), a high variability in printing quality is still observed. Here, 90° and 45°-oriented wall presents two rugosity severities. Considering a lattice thickness of 310-330µm, the down-skin effect on 45°-oriented walls creates highly severe surface defects of 70µm depth and 30µm large whereas the up-skin effect creates a very good surface aspect on these same walls. Walls oriented at $\theta=90^\circ$ present some partially melted particles but no large surface defects.

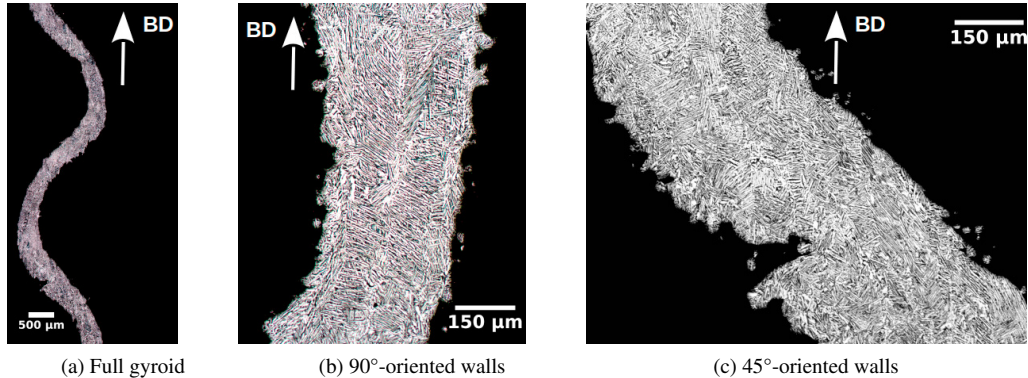


Fig. 3: Surface roughness observation on a vertical (X-BD) gyroid lattice slice (Ti-6Al-4V, SLM, HIP). Zoom in (b) vertical and (c) 45° -oriented thin-walls.

3.2. Microstructure

Image post-processing using OrientationJ analysis plugin (ImageJ) are undertaken to distinguish the microstructures features (fig. 4). TWL presents a Widmanst  tten microstructure, typical for HIPed Ti-6Al-4V manufactured by SLM, as shown figure 3. The latter presents colonar lamellar colonies oriented along the BD. Walls close to the 90° orientation present large elongated colonies, up to 120 m large and 300 m high, oriented along the wall plane (long axis parallel to the local surface). In comparison, walls oriented around 45° present thinner (~50 m) and smaller (~100 m) columnar colonies. In this configuration, thermal gradients grain growth oriented along BD results in smaler lamellar colonies which long axis is no longer allign with the wall plane. This elongated shape and the strong difference in colony size between surface volume and core volume are created with high thermal gradient along the BD direction, resulting in epitaxial growth.

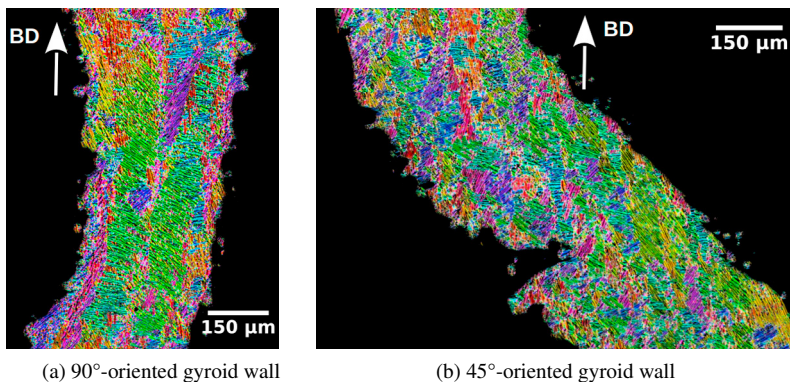


Fig. 4: Microstructure observation on a vertical (X-BD) gyroid lattice slice (Ti-6Al-4V, SLM, HIP). The applied colourisation is based on lamellas orientation Zoom in (a) vertical and (b) 45°-oriented thin-walls.

3.3. Topology and stress field heterogeneity

The gyroid FEM results show an important structure effect as normalised Crossland FIP $FIP_{CR,norm}$ (eq. 3) presents an important heterogeneous stress distribution. Highly Stressed Volumes (HSV) allow a better understanding of FIP distribution (tab. 2). For instance, V90 correspond to the volume of elements where $FIP_{CR,norm} \geq 0.9 \times FIP_{CR,norm}^{max}$, $FIP_{CR,norm}^{max}$ corresponding to the maximal normalised FIP over the TWF. Therefore, a large

part of the TWL volume undertake a load lower than V30 (37.39%), whereas a smaller volume undertake high loads (V70=11.43%, V90 = 0.64%).

Table 2: Highly Stressed Volumes (HSV) and their associated normalised stress. V90 correspond to the volume of elements where $FIP_{CR,norm} \geq 0.9 \times FIP_{CR,norm}^{max}$.

HSV	V90	V80	V70	V60	V50	V40	V30	V20	V10	V00
$FIP_{CR,norm}$	1.808	1.608	1.405	1.205	1.004	0.803	0.603	0.402	0.201	0.0
Volume[%]	0.64	3.88	11.43	24.46	36.45	48.09	62.61	75.48	90.30	100.0

The $FIP_{CR,norm}$ distribution analysis is completed with $FIP_{CR,norm}$ fields description. HSV is localised on lattice walls orientated along the loading axis (Z). Low stressed volumes are larger compared to high stressed volumes (V00-V60=75.54%), and localised in horizontal walls (0° -oriented walls).

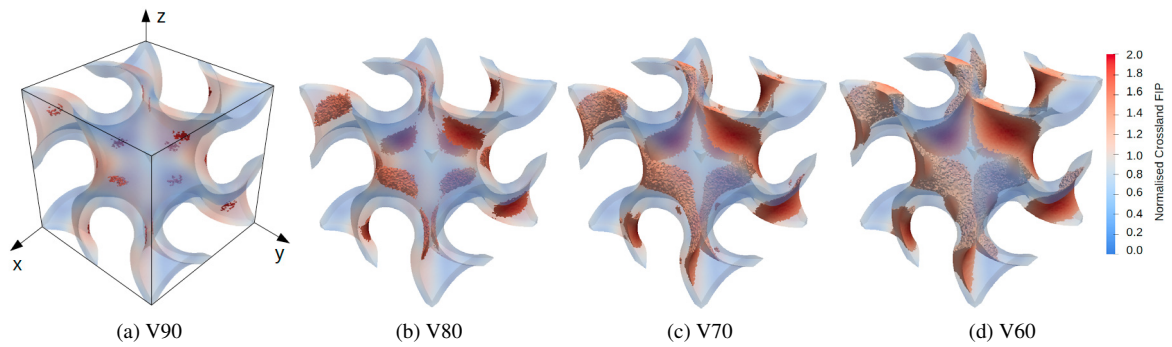


Fig. 5: Decomposition of the normalised Crossland FIP field in a gyroid thin-wall-lattice unit cell loaded along Z axis.

3.4. Discussion

We expect microstructure and surface roughness variation in gyroid TWL to present an important mechanical heterogeneity and anisotropy of HCF behaviour. Regarding the rugosity effect only, low fatigue resistance regions have been identified in misoriented walls regarding the BD. Nevertheless, the complex topology of lattices induces a highly heterogeneous loading of the TWL structure resulting in high stressed volumes localised in 90° -oriented walls along the load direction. Hence, the fatigue behaviour at the local scale is driven by the competition between surface roughness and microstructure, both having an anisotropic and heterogeneous character at the scale of the lattice VER. Therefore, it is difficult to fully understand HCF crack initiation mechanisms at the scale of the TWL. Consequently, this work investigates the heterogeneity of non-architected thin-wall specimens describing local behaviour over the gyroid structure.

4. HCF of thin-walls

4.1. Effect of thickness

The thickness effect on TWS fatigue resistance is revealed comparing TWS HCF life (uniaxial tension, 1.10^6 , $R=0.1$) for one orientation (90°) and one surface state (as-build) (tab. 3). Increasing the thickness of 90° -oriented TWS results in a decrease (-22%) of the HCF limit. In addition, while $500\mu\text{m}$ - 90° -AB TWS presents a behaviour comparable to bulk behaviour, $300\mu\text{m}$ - 90° -AB TWS shows a different behaviour displaying two sets of points (fig. 6): one set of sample without failure ($N=1.0^6$ cycles) and the other set of samples which rupture occurred around 100 000 cycles, on a wide range of normalised stresses [2,80 - 3,27].

Table 3: Thin-wall high cycle fatigue limits ($R=0.1$, $N=1.10^6$ cycles).

Thickness	$\theta=90^\circ$	$\theta=45^\circ$
300 μm	$\beta_{norm} = 2.884$	$\beta_{norm} = 1.770$
500 μm	$\beta_{norm} = 2.397$	-
Bulk	$\beta_{norm} = 2.050$	-

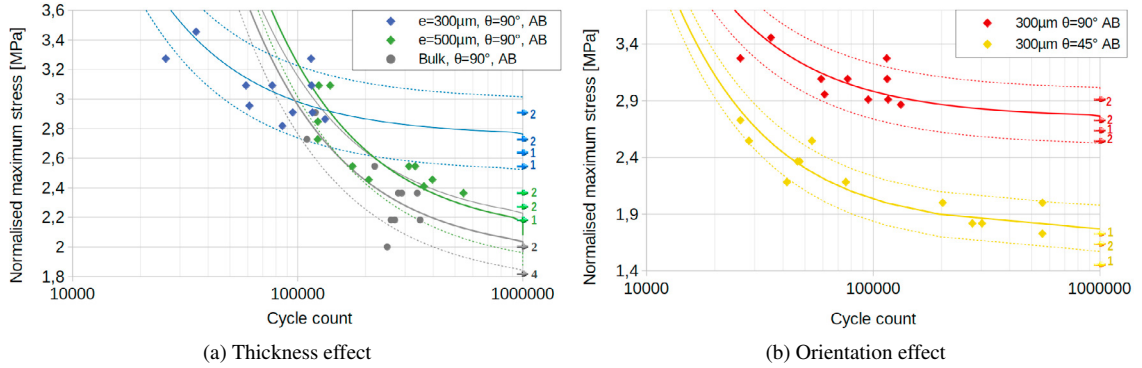


Fig. 6: Thin-wall samples whöler curves (Ti-6Al-4V, SLM, HIP, as-built).

4.2. Effect of orientation

The effect of TWS orientation on their fatigue resistance is highlighted comparing HCF behaviour with one thicknesses (300 μm) and one surface state (as-build) (fig. 6). The 45°-misorientation between TWS axis and BD results in a decrease of HCF life limit (-39%). Although the whöler curve for TWS with $\theta=45^\circ$ keep the same tendency as 90°-oriented TWS, the gap between 100 000 cycles 1.10^6 cycles in 300 μm -90°-AB results is no longer observed.

5. Discussion

- The drastic difference in HCF behaviour between 90°-oriented 300 μm and 500 μm TWS can be explained by understanding crack initiation and propagation mechanisms in Ti-6Al-4V TWS. It is known that crack initiation in lamellar Ti-6Al-4V occurs preferentially in between lamellas or at colonies boundaries. Moreover, crack initiation in bulk materials takes places at the specimen surface or sub-surface. Later, the specimen microstructure influences the very first steps of crack propagation : fine microstructure corresponding to numerous propagation obstacles results in a slower crack propagation. Considering the microstructures highlighted in figure 7, the 300 μm TWS presents large colonies compared to its wall thickness, locally reaching over 200 μm width. At variance, the 500 μm TWS exhibits thinner colonies under 60 μm width, imposing a higher amount of structural barriers on crack propagation. Consequently, the fatigue behaviour of the 500 μm -90°-AB TWS approaches the one of bulk behaviour. On the contrary, the 300 μm -90°-AB TWS might present a colony that locally cross over the wall thickness, without important structural barrier, explaining its particular HCF behaviour.
- Fatigue life is highly dependent on the presence of defects. High stress concentration at large surface defects causes a severe drop of HCF limit. This is emphasise by the TWS scale effet : the introduction of large defects compared to the low thickness can have an important detrimental influence on the FIP field distribution across the wall, resulting in a premature crack initiation.
- Although numerical simulations identified 90°-oriented regions as the most detrimental areas for HCF behaviour in TWL, the FEM calculation only takes one set of parameters into account, applying on the entire structure those of bulk material vertically manufactured. Thus, to complete the analysis, the calculated nor-

malised fatigue limits β_{norm} (tab. 3) are compared to Crossland FIP average $\overline{FIP}_{(CR,norm)}$, calculated on 90° and 45°-oriented walls in the TWS over 10% volume of the unit cell. The calculated ratios $\frac{\overline{FIP}^{90}_{(CR,norm)}}{\beta_{norm}^{90}} = 1.81$ and $\frac{\overline{FIP}^{45}_{(CR,norm)}}{\beta_{norm}^{45}} = 1.91$ present a very low difference, indicating that both 90° and 45°-orientated walls in TWL can be defined as critical region for fatigue behaviour.

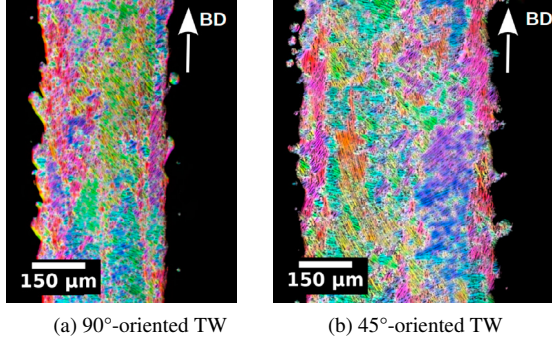


Fig. 7: Microstructure observation of vertical thin-walls (a) 300µm and (b) 500µm (Ti-6Al-4V, HIP, as-built).

6. Conclusion and prospects

HCF tests conducted on non-architected thin-walls specimens highlight a very specific fatigue behaviour strongly influenced by wall thickness as well as wall orientation regarding the build direction, resulting in a variation up to 30% of the fatigue limit. The comparison between the distribution of Crossland fatigue indicator parameter within the lattice and the non-architected thin-walls fatigue limits ($\theta=90,45^\circ$, $e=300\mu\text{m}$) clearly demonstrated that roughness and FIP distribution effects are in real competition. This results in a large critical volume for fatigue resistance covering 90° and 45° oriented regions (case of uniaxial loading along BD).

Surface roughness is probably the strongest material parameter of influence on fatigue life behaviour. Consequently, notch defect shadows all other effects. To minimise stress concentration sites, a surface treatment will be applied to suppress high K_t sites, and hence evaluate the microstructure effect and gradient effect only. Machining is not possible on complexe strucutres, neither on tubular thin-wall specimens. Therefore, a chemical polishing will be applied.

Also, it has been demonstrated that stress gradient enhance fatigue life resistance. The complexe topology of thin-wall lattices introduce by nature high stress gradient within the small thickness of its walls. Gradient localisation and the characterisation of their effect on HCF allow a better description of the loading complexity and fatigue response.

References

- Hannibal, M., Knight, G., 2018. Additive manufacturing and the global factory: Disruptive technologies and the location of international business. *International Business Review*, 27, 1116 – 1127.
- Yuan, L., Ding, S., Wen, C., 2019. Additive manufacturing technology for porous metal implant applications and triple minimal surface structures: A review. *Bioactive Materials*, 4, 56 – 70.
- Masuo, H., Tanaka, Y., Morokoshi, S., Yagura, H., Uchida, T., Yamamoto, Y., Murakami, Y., 2017. Effects of Defects, Surface Roughness and HIP on Fatigue Strength of Ti-6Al-4V manufactured by Additive Manufacturing. *Procedia Structural Integrity*, 7, 19 – 26.
- Tammas-Williams, S., Withers, P. J., Todd, I., Prangnell, P. B., 2017. The Influence of Porosity on Fatigue Crack Initiation in Additively Manufactured Titanium Components. *Scientific Reports*, 7, 1 – 13.
- Stef, J., Poulon-Quintin, A., Redjaimia, A., Ghanbaja, J., Ferry, O., 2018. Mechanism of porosity formation and influence on mechanical properties in selective laser melting of Ti-6Al-4V parts. *Materials and Design*, 156, 480 – 493.
- Vaysette, B., 2020. Comportement en fatigue de pièces de Ti-6Al-4V obtenues par SLM et EBM : effet de la rugosité. Phd, Ecole Nationale Supérieure d'Arts et Métiers (France).

- Speirs , M., Van Hooreweder , B., Van Humbeeck , J. et Kruth , J. P., 2017. Fatigue behaviour of NiTi shape memory alloy scaffolds produced by SLM, a unit cell design comparison. *Journal of the Mechanical Behavior of Biomedical Materials* 70, 53–59
- Attaran , M. (2017). The rise of 3-D printing : The advantages of additive manufacturing over traditional manufacturing. *Business Horizons* 60, 677 – 688
- Dallago, M., Winiarski, B., Zanini, F., Carmignato, S., Benedetti, M., 2019. On the effect of geometrical imperfections and defects on the fatigue strength of cellular lattice structures additively manufactured via Selective Laser Melting. *International Journal of Fatigue*, 124, 348 – 360.
- Gu , D. D., Meiners, W., Wissenbach, K. et Poprawe , R., 2012. Laser additive manufacturing of metallic components : Materials, processes and mechanisms. *International Materials Reviews* 57, 133 – 164
- Kaur, I., Singh, P., 2021. Critical evaluation of additively manufactured metal lattices for viability in advanced heat exchangers. *International Journal of Heat and Mass Transfer*, 168.
- Innocentini, M., Botti, R., Bassi, P., Paschoalato, C., Flumignan, D., Franchin, G., Colombo, P., 2019. Lattice-shaped geopolymmer catalyst for biodiesel synthesis fabricated by additive manufacturing. *Ceramics International*, 45, 1443 – 1446.
- Xiang, J., Du, J., 2019. Energy absorption characteristics of bio-inspired honeycomb structure under axial impact loading. *Materials Science and Engineering*, 696, 283 – 289.
- Yang, E., Leary, M., Lozanovski, B., Downing, D., Mazur, M., Sarker, A., Khorasani, A. M., Jones, A., Maconachie, T., Bateman, S., Easton, M., Qian, M., Choong, P. et Brandt, M., 2019. Effect of geometry on the mechanical properties of Ti-6Al-4V Gyroid structures fabricated via SLM : A numerical study. *Materials and Design* 165, 184 – 108.
- Refai, K., 2020. Effet de la méso-architecture sur le comportement en fatigue des structures lattices optimisées obtenues par fabrication additive. Phd, Ecole Nationale Supérieure d'Arts et Métiers (France).
- Bobbert , F. S., Lietaert , K., Eftekhari , A. A., Pouran , B., Ahmadi , S. M., Weinans , H. et Zadpoor , A. A., 2017. Additively manufactured metallic porous biomaterials based on minimal surfaces : A unique combination of topological, mechanical, and mass transport properties. *Acta Biomaterialia* 53, 572–584
- Refai , K., Brugger , C., Montemurro , M. et Saintier , N., 2019. "Multi-axial fatigue behaviour of titanium periodic cellular structures produced by Selective Laser Melting (SLM)", MATEC Web of Conferences, 300 – 304
- Yang, L., Yan, C., Cao, W., Liu, Z., Song, B., 2019. Compression–compression fatigue behaviour of gyroid-type triply periodic minimal surface porous structures fabricated by selective laser melting. *Acta Materialia*, 181, 49 – 66.